Journal of Applied Polymer Science

# Bright Field and Dark Field STEM-IN-SEM Imaging of Polymer Systems

**Binay Patel, Raymond Pearson, Masashi Watanabe**
Department of Materials Science and Engineering, Lehigh University, Bethlehem, Pennsylvania 18015
Correspondence to: M. Watanabe (E-mail: masashi.watanabe@lehigh.edu)

**ABSTRACT:** The microstructural analysis of polymer systems (e.g., polymers and their composites) has largely been conducted by transmission electron microscopy (TEM). However, hard materials (e.g., metals and ceramics) are better suited for TEM imaging because such materials can withstand the high energy electron beam generated in TEM instruments. Recently, scanning TEM in scanning electron microscopy (STEM-IN-SEM) has emerged as a viable alternative to TEM imaging of polymer systems. STEM-IN-SEM uses a versatile and user-friendly SEM instrument for examining the microstructure of polymer systems. In this study, we outline our method for STEM-IN-SEM imaging and apply it to the imaging of various commercial and model polymer systems. Imaging results are evaluated on the basis of measured signal intensity, which compare favorably to microstructural analysis using more costly TEM and STEM instruments. Furthermore, these comparable signal intensities are achieved through STEM-IN-SEM imaging with specimens that are three times thicker than those required for conventional TEM imaging. In this respect, as compared to TEM, STEM-IN-SEM offers faster specimen preparation times coupled with easier usability and lower maintenance costs, which are all attractive attributes for efficient quality control measures in industry. © 2014 Wiley Periodicals, Inc. J. Appl. Polym. Sci. **2014**, *131*, 40851.

**KEYWORDS:** composites; microscopy; morphology; nanoparticles; thermosets

Received 4 February 2014; accepted 13 April 2014
**DOI: 10.1002/app.40851**

## INTRODUCTION

Characterization of polymer systems by transmission electron microscopy (TEM) and scanning TEM (STEM) has been limited by specimen contamination and damage due to high energy electron beams (e.g., 200 keV).[1] The strengths of microstructural analysis via TEM/STEM include high-resolution electron diffraction studies and knowledge of elemental composition through X-ray analysis. However, these strengths are not advantageous for most polymer systems. Polymer systems typically lack long-range ordered structures, making electron diffraction studies difficult. In addition, polymer systems are typically comprised mostly of carbon, oxygen, and hydrogen, elements that are not favorable for quantitative X-ray analysis. While heavy metal staining of polymer systems may improve image contrast during TEM/STEM observation, such stains are toxic and may change the chemical structure of polymer systems.[2] Therefore, the primary route for the microstructural characterization of polymer systems is through scanning electron microscopy (SEM) of bulk samples. SEM instruments provide surface morphology and elemental distributions with relatively lower energy electrons, lower acquisition, and maintenance costs, along with more user-friendly operation than TEM/STEM instruments.

A technique for the microstructural analysis of a thin specimen, as opposed to the bulk sample, would make SEM the definitive choice for electron microscopy-based studies of polymer systems. Scanning TEM in SEM (STEM-IN-SEM)[3] has emerged as a suitable characterization tool for polymer systems. Typically, STEM-IN-SEM uses an electron-transparent thin specimen and an electron detector placed underneath the specimen to mimic the operation of STEM instruments. The resulting images display bright-field (BF) signals in which the primary electron beam penetrates the specimen, and then the on-axis electron detector collects the subsequently transmitted electrons. Just as in TEM/STEM, BF STEM-IN-SEM images form mass-thickness contrast with signal intensity dependent on both the mass of the constituents in a specimen and the actual specimen thickness. Many microscope configurations for STEM-IN-SEM have been developed for BF imaging.[4–10] Recently, using the lower voltage electron beam, larger field of view and exclusion of postspecimen projection lens in a SEM instrument, BF STEM-IN-SEM imaging has shown results similar to BF TEM observation of polymer morphology.[11] BF STEM-IN-SEM imaging has been successfully applied to microstructural observation of various polymer-based latex particles,[12] particle size, and distribution analysis,[13] and X-ray elemental mapping of soft materials.[14]

BF imaging is sufficient for analyzing particle size and distribution but its dual contrast dependence (to both mass and thickness) limits image interpretability. In comparison, high angle dark-field (DF) imaging in which the signal intensity is directly

related to Rutherford scattering of electrons (and hence dependent on atomic number) produces more easily interpretable images. In DF images, higher signal intensity correlates to heavier atomic number, and vice versa. Therefore, image contrast in this method is called *Z*-contrast and has been traditionally developed in STEM instruments. Development of STEM-IN-SEM for DF imaging[4,9,15,16] has often included complex instrument configurations or required expensive electron detectors. Recently, a simple STEM-IN-SEM holder for both BF and DF imaging has been developed by some of the authors. Details on the design, theoretical construct and optimization of imaging conditions for the use of this specimen holder in a Hitachi 4300 SEM can be found elsewhere.[17] While our current design has only been tested in a Hitachi 4300 SEM, it should be readily adapted to be used in any modern SEM instrument.

New SEM instruments are generally more affordable acquisitions as compared to new TEM/STEM instruments. Consequently, SEM instruments have been widespread for daily materials characterization in industry. Nevertheless, TEM/STEM imaging provides researchers with advantageous methods of characterizing the microstructure of materials. Specifically for the polymer industry it may now be possible to close the imaging gap between SEM and TEM/STEM instruments. Typically, polymer systems use secondary phase(s) that are on the nanometer scale or larger. Without the need for atomic scale resolution, a strong suit of TEM/STEM instruments, modern SEM instruments provide sufficient resolution for microstructural characterization. Therefore, the goal of this study is to compare the use of our BF and DF STEM-IN-SEM imaging technique as a low cost alternative to TEM/STEM imaging of polymer systems at the nanometer scale. The imaging potential of our technique will first be demonstrated for various polymer systems followed by qualitative and quantitative comparisons with TEM/STEM imaging.

## EXPERIMENTAL

### Instruments

A Hitachi 4300 field-emission SEM equipped with a transmission electron (TE) detector and a yttrium–aluminum–garnet (YAG) detector were used for BF and DF STEM-IN-SEM imaging throughout this study. Typical operating conditions for BF and DF STEM-IN-SEM imaging include an accelerating voltage of 30 kV, a probe current of 25 pA and a working distance of 4.6 mm.

In this particular microscope configuration, a TE detector is located below the specimen chamber and used for BF image collection. A YAG detector, typically positioned directly above a bulk sample for backscattered-electron imaging, is instead positioned off-axis and at the same height as a thin specimen to allow for DF signal collection. A thin-sectioned specimen is placed on a TEM copper grid and secured within a specimen housing at the top of the STEM-IN-SEM holder. As a scanning electron beam penetrates the specimen, electrons are scattered at various angles, depending on the elemental composition across the specimen. A gold-coated inclined copper plate with a center hole facilitates BF and DF image formation. Electrons scattered at lower-angles, defined as <55 mrad (corresponding to the cut-off angle of the center hole on the inclined plate), pass through the center hole opening and are collected by the TE detector to produce BF images. Electrons scattered at higher-angles (>55 mrad) are deflected off of the inclined plate and collected by the YAG detector for DF image formation.

Comparative TEM characterization for select specimens was conducted in a JEOL 2000FX TEM instrument operated at an accelerating voltage of 200 kV. Comparative STEM analysis on select specimens was carried out in an aberration-corrected JEOL JEM-ARM 200CF STEM instrument operated at an accelerating voltage of 60 kV.

### Materials

In this study, a variety of commercial and model polymer systems were investigated. Two commonly available commercial polymer systems were examined: 0.3 μm (diameter) polystyrene latex particles (Ted Pella) and pellets of high-impact polystyrene (HIPS; Nova Chemicals 702-H2N). One droplet of polystyrene latex particles (from aqueous solution) was placed on a standard holey carbon TEM grid for use during imaging. All model polymer systems used a diglycidyl ether of bisphenol A (DGEBA) epoxy (DER 331 resin from Dow Chemical Co.) as the matrix material. The choice of epoxy as the matrix material was twofold: (1) epoxy-based composites enjoy widespread use as adhesives and encapsulants in the consumer electronics industry and (2) the use of a common matrix between specimens would highlight the contrast variations when various types of second phase particles are imaged. The DGEBA epoxy-based composites investigated included 10 wt % 23 nm (diameter) silica nanoparticles (3*M*) in DGEBA epoxy, 18 wt % carboxyl-terminated liquid butadiene-acrylonitrile (CTBN rubber) reactive oligomer (Hycar 1300×8 from Emerald Performance Chemicals Co.) and 5 wt % 23 nm (diameter) silica (3*M*) in DGEBA epoxy, 2.5 phr triblock copolymer of polystyrene, 1,4-polybutadiene and syndiotactic poly(methyl methacrylate) (SBM; Nanostrength E20 from Arkema) in DGEBA epoxy and 25 phr SBM in DGEBA epoxy.

All epoxy-based materials were cured with piperidine (5 phr) for 6 h at 160°C. A few points should be made here regarding the cure schedule. A cure temperature of 160°C was chosen to ensure matrix ductility as well as minimize particle size generated when block copolymers are used. Using another cure temperature the microstructure of the secondary phases in these polymer systems would change. However, the size of the resultant microstructures would not fall below the resolution limit of modern SEM instruments, thereby enabling the use of BF and DF STEM-IN-SEM imaging for these (and largely all) polymer systems.

All samples were cryo-ultramicrotomed to a specimen thickness of 100 nm. Select specimens containing a butadiene phase (e.g., HIPS and composites containing CTBN and SBM) were stained with osmium tetroxide ($OsO_4$), which preferentially stains the butadiene segments of these phases for higher contrast during imaging.

Stained specimens of 25 phr SBM (Arkema) in DGEBA epoxy were used for comparison to TEM imaging. Furthermore,

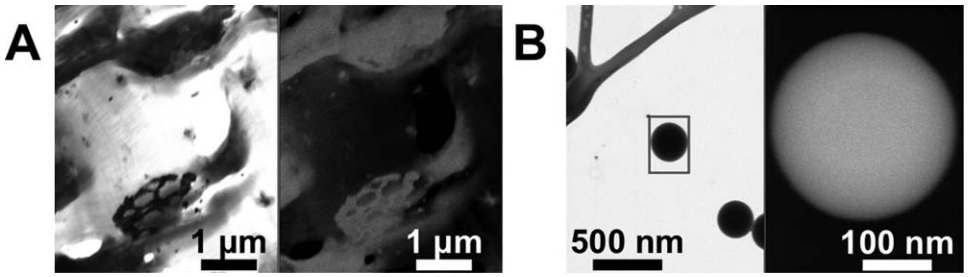


**Figure 1.** BF and DF STEM-IN-SEM images taken at 30 kV of various commercial polymer systems: (a) HIPS (BF ×10,000 [left], DF ×10,000 [right]) and (b) 0.3 μm (diameter) polystyrene latex particles (BF ×40,000 [left], DF ×200,000 [right]). The DF image in (b) is scanned over the inset region within the corresponding BF image.

unstained specimens of 10 wt % 23 nm (diameter) silica (3*M*) in DGEBA epoxy were used for comparison to STEM imaging.

To investigate the effect of specimen thickness on image quality, unstained specimens of 25 phr E20 SBM in DGEBA epoxy were cryo-ultramicrotomed to the following thicknesses: 50, 100, 150, and 300 nm. Two sets of electron-transparent specimens were prepared for each thickness. The first set of specimens was observed by TEM with an accelerating voltage of 200 kV. The second set was observed by BF STEM-IN-SEM with an accelerating voltage of 30 kV. The measured signal intensity from each set of images (collected at 20,000×) was analyzed using Image J software.[18] The measured signal intensity as a function of specimen thickness is compared between both microscopy techniques.

## RESULTS AND DISCUSSION

### Morphological Analysis Using BF and DF STEM-IN-SEM Imaging

**Commercial Polymer Systems.** BF and DF STEM-IN-SEM images were successfully acquired from $OsO_4$-stained HIPS and 0.3 μm (diameter) polystyrene latex particles [Figure 1(a,b)]. The discrete polybutadiene phase in HIPS is stained preferentially with $OsO_4$. Due to the heavy metal staining, the polybutadiene phase is dark in BF, while the less-massive polystyrene matrix appears brighter. The brightest regions in the BF image represent holes in the specimen. The DF image of HIPS displays complementary contrast. The $OsO_4$-stained discrete phase (effective $Z = 28$, due to the heavy-metal staining) scatters electrons to higher angles than the unstained matrix (effective $Z = 3.7$). Therefore, the polybutadiene phase appears brighter than the polystyrene matrix in the DF image. The darkest regions in the DF image represent holes in the specimen since no electrons were scattered from these areas. Similarly, the 0.3 μm (diameter) polystyrene latex particles (effective $Z = 3.5$) are dark in BF but bright in DF as shown in Figure 1(b). The BF image shows slight contrast variations across the particles due to particle geometry. Such contrast variation is less prevalent in the DF image, except for the edge of the particle, as the contrast is more atomic number dependent.

**Model Polymer Systems.** The same approach was applied to imaging model polymer systems (Figure 2). For the filled epoxy system consisting of 10 wt % 23 nm (diameter) silica nanoparticles, the discrete silica phase appears dark in BF images because these nanoparticles are more massive than the epoxy matrix [Figure 2(a)]. It is worth noting that some silica nanoparticles appear darker than others, highlighting the inconsistent interpretability of BF images. The DF image shows *Z*-contrast for which the scattering from the discrete silica phase [effective $Z = 10$, Figure 2(a)] leads to higher electron signals reaching the off-axis YAG detector as compared to the lower atomic number epoxy matrix (effective $Z = 3.7$).

The hybrid epoxy system consists of 18 wt % $OsO_4$-stained CTBN rubber and 5 wt % 23 nm (diameter) silica nanoparticle [effective $Z = 28$ and effective $Z = 10$, respectively, Figure 2(b)]. As shown in the DF image, both the $OsO_4$-stained CTBN rubber phase and the discrete silica phase scatter more electrons than the epoxy matrix. While both discrete phases display low contrast in BF, these phases display different contrast in DF; the silica phase displays lower signal intensity owing to its lower effective *Z* compared to the $OsO_4$-stained CTBN phase.

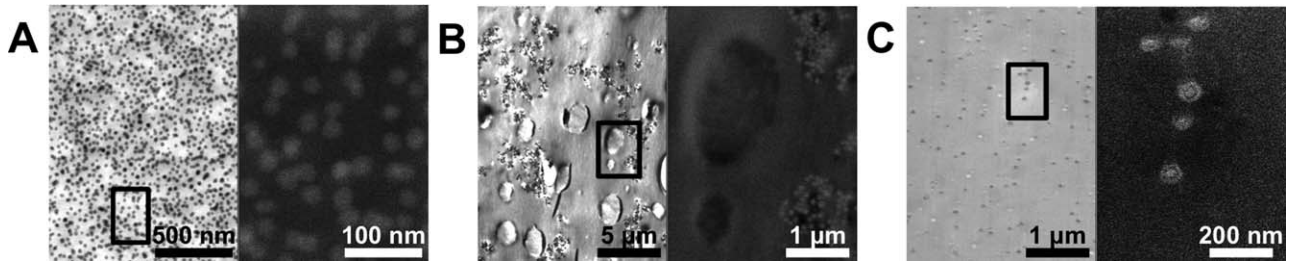


**Figure 2.** BF and DF STEM-IN-SEM images taken at 30 kV of various model polymer systems: (a) 10 wt % 23 nm (diameter) silica in DGEBA epoxy (BF ×50,000 [left], DF ×250,000 [right]), (b) $OsO_4$-stained 18 wt % CTBN and 5 wt % 23 nm (diameter) silica in DGEBA epoxy (BF ×4000 [left], DF ×20,000 [right]), and (c) $OsO_4$-stained 2.5 phr SBM in DGEBA epoxy (BF ×20,000 [left], DF ×100,000 [right]). The DF images for each system are scanned over the inset regions within the corresponding BF images.

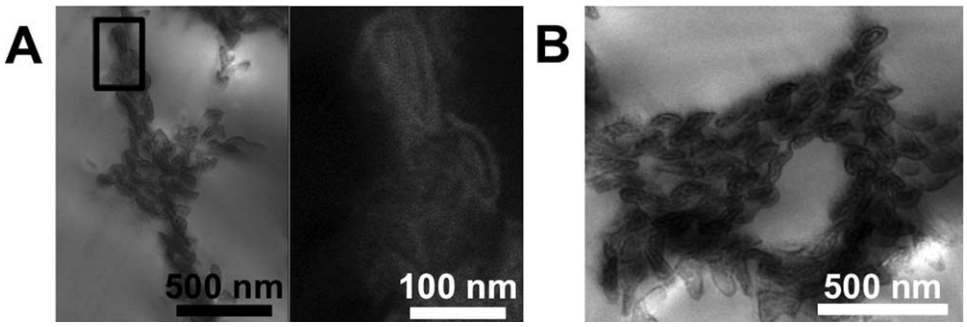


**Figure 3.** Images of $OsO_4$-stained 25 phr SBM in DGEBA epoxy: (a) BF (left, ×50,000) and DF (right, ×250,000) STEM-IN-SEM images taken at 30 kV (the DF image is scanned over the inset region within the BF image) and (b) BF TEM image (×100,000).

The rubber nanoparticle-modified epoxy consists of 2.5 phr $OsO_4$-stained SBM [effective $Z = 28$, Figure 2(c)]. While the DF image is noisy, it clearly shows the two components of the SBM phase that are immiscible with the epoxy matrix, namely the $OsO_4$-stained butadiene phase and the darker styrene phase. The methyl methacrylate phase is miscible with the epoxy matrix and cannot be distinguished.

### BF STEM-IN-SEM Imaging Versus BF TEM Imaging

**Imaging Quality.** BF and DF STEM-IN-SEM images of $OsO_4$-stained 25 phr SBM-modified epoxy are shown in Figure 3(a). Significant agglomeration of the discrete SBM phase can be seen within the epoxy matrix (attributed to the high SBM content). Through DF imaging, the microstructure of the discrete phase may be distinguished on the nanometer scale. The preferentially $OsO_4$-stained polybutadiene component of the discrete SBM phase appears bright and surrounds the unstained polystyrene component, which appears dark [right side of Figure 3(a)]. A BF TEM image of the same $OsO_4$-stained 25 phr SBM in DGEBA specimen [Figure 3(b)] shows comparable quality to the BF STEM-IN-SEM image. However, the higher energy electron beam (200 keV) causes specimen damage [as evident from the bottom regions of Figure 3(b)]. During STEM-IN-SEM imaging, the effects of the lower energy electron beam (30 keV) are not as severe. As the knock-on damage threshold for carbon is approximately 80 keV,[19] the lower energy electron beam used in STEM-IN-SEM is suitable for carbon-based materials such as polymer systems.

Furthermore, the principle advantage of STEM-IN-SEM over TEM is in the efficient acquisition of DF images. Normally, DF imaging in TEM requires low-angle Bragg reflections of electrons in a specimen to produce images with diffraction contrast. However, neither amorphous nor semicrystalline polymer systems produce strong electron diffraction because these materials do not possess long-range ordered structures. Therefore, no periodic reciprocal lattice is formed for DF TEM imaging. Thus, DF TEM images of polymer systems, such as stained 25 phr SBM in DGEBA, is not practical unless an annular objective aperture is used.[20] The newly developed specimen holder for BF and DF STEM-IN-SEM allows for the collection of annular DF signals by separating high-angle and low-angle scattered electrons.[17]

A more comprehensive comparison of DF STEM-IN-SEM imaging may be performed with high-angle annular DF (HAADF) STEM imaging, since both imaging techniques show *Z*-contrast. BF and DF STEM-IN-SEM images of unstained 10 wt % 23 nm (diameter) silica nanoparticles in DGEBA are shown in Figure 4(a). The higher magnification DF image displays *Z*-contrast and allows for effective particle size measurements of the silica phase, which appears bright in comparison to the low atomic number of the epoxy matrix. HAADF STEM imaging of the unstained 10 wt % 23 nm (diameter) silica in epoxy [Figure 4(b)] produces comparable imaging results, albeit on a STEM instrument that is more expensive and harder to operate than a SEM instrument. The HAADF STEM image does display higher contrast, compared to the DF STEM-IN-SEM image, owing to the higher signal-to-background ratios produced by aberration-corrected fine electron probes. Conversely, electron probes refined by aberration correction result in higher current density that can lead to significant surface contamination especially in unstained carbon-based materials. Indeed, evidence of the onset

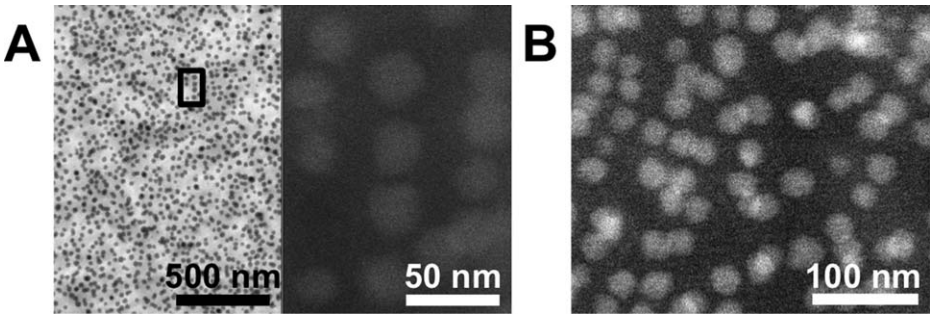


**Figure 4.** Images of 10 wt % 23 nm (diameter) silica in DGEBA epoxy: (a) BF (left, ×50,000) and DF (right, ×500,000) STEM-IN-SEM images taken at 30 kV (the DF image is scanned over the inset region within the BF image) and (b) HAADF STEM image (×600,000).

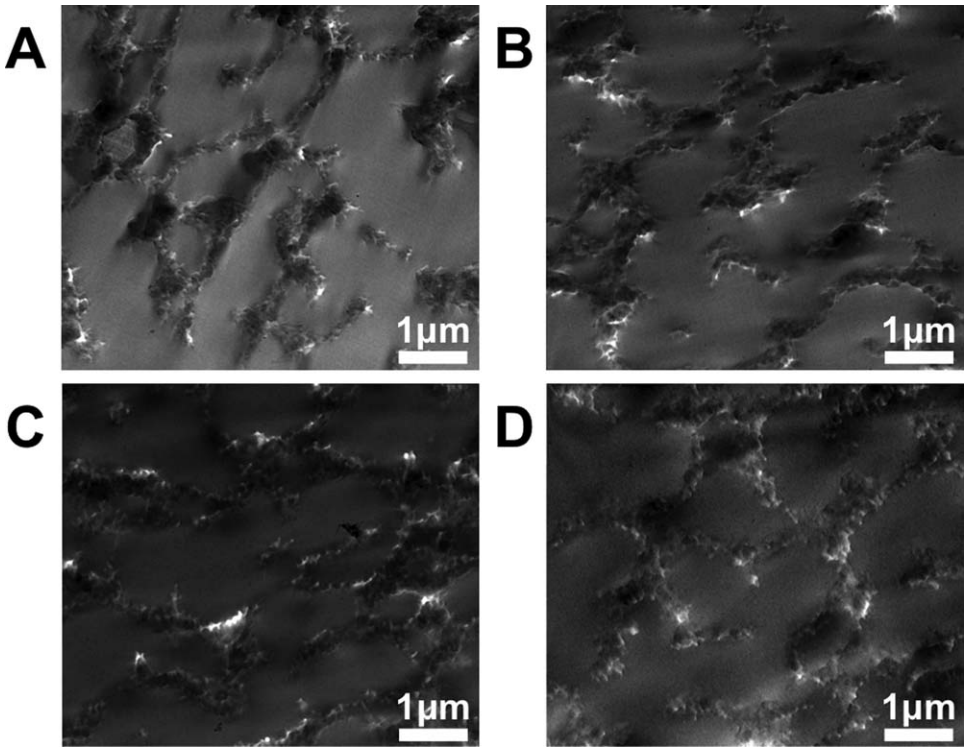


**Figure 5.** BF TEM images (×20,000) taken at 200 kV of unstained 25 phr SBM in DGEGA epoxy at various specimen thicknesses: (a) 50, (b) 100, (c) 150, and (d) 300 nm.

of surface contamination is present in the reduced image quality observed in the top right region of the HAADF STEM image of unstained 10 wt % 23 nm (diameter) silica in epoxy [Figure 4(b)]. Such evidence of surface contamination effects is not present in the lower-contrast DF STEM-IN-SEM image of the same unstained system.

**Influence of Specimen Thickness on Signal Intensity.** BF TEM images of unstained 25 phr SBM in epoxy (Figure 5), obtained with an accelerating voltage of 200 kV, yielded diminishing mean signal intensity with increasing specimen thickness. The mean signal intensity decreased from nearly 100 gray levels (GL) to nearly 70 GL, as the thickness of the specimen increased from 50 to 300 nm (Figure 6). Usually BF TEM imaging is performed with parallel illumination of electrons onto a specimen. When a specimen is thin (e.g., 100 nm or less), single scattering events occur on the electron beams interaction with the specimen, and subsequent signal intensity displays mass–thickness contrast. However, as the specimen thickness increases, the electron beam must penetrate through more material, which increases the likelihood of plural scattering events. Plural scattering events through low-angle electron scattering lead to a broader distribution of transmitted electrons leaving the specimen. After passing through postspecimen projection lenses, which are common in TEM instruments, these transmitted electrons reach the detector with signal intensity that is broader than the signal intensity distribution produced from transmitted electrons emitted from thinner specimens. Therefore, the mean signal intensity decreases as the specimen thickness increases, as observed. The measured decrease in mean signal intensity during BF TEM imaging in this study may indicate a gentle decline in the mean signal intensity for the range of specimen thicknesses observed.

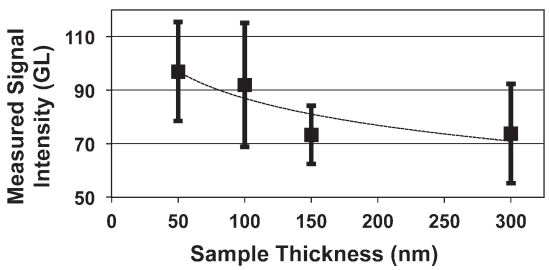


**Figure 6.** Measured BF TEM signal intensity as a function of specimen thickness.

During BF STEM-IN-SEM imaging of the unstained 25 phr SBM in epoxy (Figure 7), conducted at an accelerating voltage of 30 kV, the mean signal intensity increased from nearly 120 GL to nearly 150 GL, as the thickness of the specimen increased from 50 to 150 nm (Figure 8). At specimen thicknesses greater than 150 nm, the mean signal intensity dropped to nearly 120 GL as measured at a specimen thickness of 300 nm. At an accelerating voltage of 30 kV, the mean free path for single scattering of electrons traveling through carbon is 54 nm, obtained using an approximation.[19] Therefore, plural scattering is present for the specimens with specimen thicknesses of 100, 150, and 300 nm observed in this portion of the study.

It is surprising that the experimental signal intensity results from the BF STEM-IN-SEM images show an increase in mean

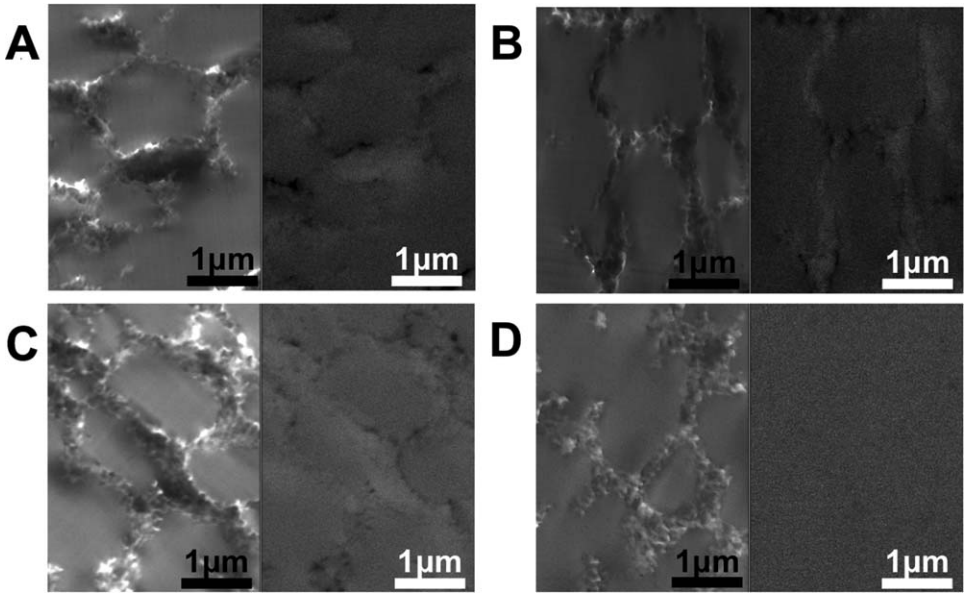


**Figure 7.** BF (left, ×20,000) and DF (right, ×20,000) STEM-IN-SEM images taken at 30 kV of unstained 25 phr SBM in DGEGA epoxy at various specimen thicknesses: (a) 50, (b) 100, (c) 150, and (d) 300 nm.

signal intensity, as the specimen thickness increases from 50 to 150 nm. Typically, a gentle decline in mean signal intensity with respect to increasing specimen thickness is expected, similar to the behavior observed during BF TEM imaging (Figure 6). Thicker specimens impede electron penetration, resulting in reduced signal intensities reaching the electron detector. Bals et al.[20] used an annular objective aperture in a TEM instrument, operated at an accelerating voltage of 150 kV, to show that the annular DF signal intensity increases with specimen thickness (up to the tens of nanometer range). In the current experiment via BF STEM-IN-SEM imaging, a similarly positive relationship between signal intensity and specimen thickness is observed up to the low 100 nm specimen thickness range.

This trend can be caused by the geometry between the specimen-holder and BF detector in the current STEM-IN-SEM setting. Even in polymer systems, in which long-range ordered structures do not exist, short-range ordered structure (e.g., a relatively similar first-nearest neighbor distance) commonly appear as a halo pattern in electron diffraction. In conventional BF TEM imaging, a relatively small objective aperture is placed around the direct electron beam to exclude

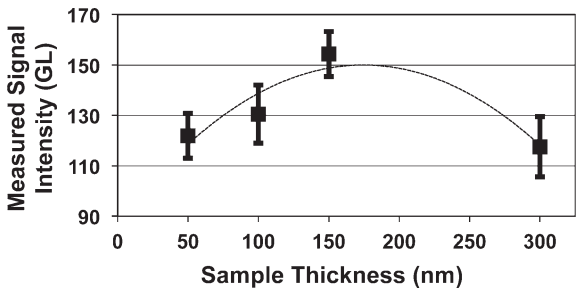


**Figure 8.** Measured BF STEM-IN-SEM signal intensity as a function of specimen thickness.

electron diffraction contributions including the first-nearest neighbor halo. In this study, a 30 μm objective aperture (equivalent to an incident probe forming angle of 3.2 mrad) was used for STEM-IN-SEM imaging. For true BF imaging, the size of the cut-off aperture on the inclined plate, which separates electron signals used for BF and DF STEM-IN-SEM imaging, should ideally be set to slightly larger than 3.2 mrad to effectively remove all diffraction contributions (similar to the conventional BF TEM imaging case). However, in our holder geometry, it is more important to use a larger enough cut-off aperture on the inclined plate to minimize diffraction contrast and to ensure pure *Z*-contrast in DF STEM-IN-SEM imaging. In the current holder geometry, the size of cut-off aperture is 55 mrad, which is much larger than the probe-forming angle. Therefore, the BF STEM-IN-SEM images obtained in this study are not formed only with pure BF signals but with both direct and deflected electron signals. The incremental increase in mean BF signal intensity from 50 to 150 nm specimen thickness range can be caused by the inclusion of deflected electron signals (e.g., from the first-nearest neighbor halo synonymous with most polymer materials). It should be noted that the underlying mass–thickness contrast in BF STEM-IN-SEM images is not significantly influenced by the inclusion of some deflected electron signals, as shown in Figure 8.

Beyond specimen thicknesses of 150 nm, there is a competition between electron penetration power and specimen thickness. At 30 keV, electrons have greater interaction with a specimen due to lower penetration power, as compared to 200 keV electrons. Therefore, after the electron beam interacts with a specimen, more high-angle electron scattering occurs at 30 keV than at 200 keV.[21] However, as the specimen becomes sufficiently thick, the low penetration power of 30 keV electrons hinders the ability of electrons to readily transverse the specimen thereby

increasing their susceptibility to signal broadening due to multiplicative plural scattering events. As a result, the mean signal intensity decreases as the specimen thickness approaches 300 nm, as observed.

Using the current imaging approach, specimens may be sectioned down to 150 nm, instead of the 100 nm required for BF TEM imaging, to enhance signal intensities during BF imaging. If only comparable signal intensities are required, specimens may only need to be sectioned to 300 nm, three times thicker than required for conventional BF TEM imaging. Any reduction in specimen preparation time effectively increases the throughput for specimen analysis. It is worth noting that signal intensities from DF STEM-IN-SEM imaging diminish with increasing specimen thickness (as seen in Figure 7). Thus, a compromise must be made during specimen preparation depending on the imaging needs of the experiment at hand.

To produce mean signal intensities on the order of those found with BF TEM imaging, BF STEM-IN-SEM imaging requires an order of magnitude more electrons. In general, the current density (per pixel) is higher in BF STEM-IN-SEM imaging as compared to BF TEM imaging, for example, $2.46 \times 10^2$ and $1.25 \times 10^{-4}$ pA/pixel$^2$, respectively, for this study. The current density for BF STEM-IN-SEM imaging is confined within a 1.8 nm diameter probe, whereas during BF TEM imaging (under parallel illumination) the current density is spread over a larger area consisting of a diameter of 6.5 μm. Thus, $1.8 \times 10^4$ electrons/pixel$^2$ take part in image formation for BF STEM-IN-SEM imaging compared to $1.8 \times 10^3$ electrons/pixel$^2$ during BF TEM imaging. Conversely, faster acquisition dwell times (per pixel) are preferred for STEM-IN-SEM imaging to deter specimen damage through localized surface heating, due to the confined electron probe used for imaging. The versatility of SEM instruments enables a range of scanning speeds to be used to determine the best conditions for the particular specimen under investigation.

## CONCLUSION

BF and DF STEM-IN-SEM imaging is a new technique for the microstructural analysis of polymers systems. BF STEM-IN-SEM images display mass–thickness contrast, while DF STEM-IN-SEM images display *Z*-contrast for polymer systems. In this study, this new technique was used for the imaging of various commercial and model polymer systems. BF and DF STEM-IN-SEM imaging is a cost-efficient alternative to BF TEM and HAADF STEM imaging for observing the microstructure of polymer systems. Furthermore, this technique reduces specimen preparation time by enabling polymer specimens to be imaged with specimen thicknesses that are three times larger than the thickness requirements for conventional BF TEM imaging. The mean signal intensity for thicker specimens observed with BF STEM-IN-SEM exceeded that of thinner specimens observed in BF TEM for a model unstained polymer system. Using BF and DF STEM-IN-SEM imaging, the potential exists for the microstructural observation of unstained polymer systems, a long-standing goal for electron microscopy studies of these materials.

## ACKNOWLEDGMENTS

The authors thank Dr. Gregory Hendricks from the University of Massachusetts Medical School (Worchester, MA) for cryoultramicrotoming the polymer systems used in this study. In addition, the authors thank Mr. William Mushock and Dr. Robert Keyes from Lehigh University (Bethlehem, PA) for valuable discussion during this study.

## REFERENCES

1. Willams, D. B.; Carter, C. B. Transmission Electron Microscopy A Textbook for Material Science; Springer: New York, **2009**.
2. Libera, M. R.; Egerton, R. F. Advances in the transmission electron microscopy of polymers. *Polym. Rev.* **2010**, *50*, 321.
3. Joy, D. C.; Maher, D. M. Is STEM possible in a SEM. *Scan. Electron Microsc.* **1976**, *1*, 361.
4. Crawford, B. J.; Liley, C. R. W. A simple transmission stage using the standard collection system in the scanning electron microscope. *J. Phys. E: Sci. Instrum.* **1970**, *3*, 461.
5. Woolf, R. J.; Joy, D. C.; Tansley, D. W. A transmission stage for the scanning electron microscope. *J. Phys. E: Sci. Instrum.* **1972**, *5*, 230.
6. Oho, E.; Baba, M.; Baba, N.; Muranaka, Y.; Sasaki, T.; Adachi, K.; Osumi, M.; Kanaya, K. The conversion of a field-emission scanning electron microscope to a high-resolution, high-performance scanning transmission electron microscope, while maintaining original functions. *J. Electron Microsc. Tech.* **1987**, *6*, 15.
7. Oho, E.; Sasaki, T.; Adachi, K.; Muranaka, Y.; Kanaya, K. An inexpensive and highly efficient device for observing a transmitted electron image in SEM. *J. Electron Microsc. Tech.* **1987**, *5*, 51.
8. Vanderlinde, W. E.; Ballarotto, V. W. Microscopy at the Nanoscale. In ISTFA 2004: 30th International Symposium for Testing and Failure Analysis, Boston, MA, **2004**; p 1.
9. Merli, P. G.; Morandi, V. Low-energy STEM of multilayers and dopant profiles. *Microsc. Microanal.* **2005**, *11*, 97.
10. Bogner, A.; Jouneau, P. H.; Thollet, G.; Basset, D.; Gauthier, C. A history of scanning electron microscopy developments: Towards "wet-STEM" imaging. *Micron* **2007**, *38*, 390.
11. Guise, O.; Strom, C.; Preschilla, N. STEM-in-SEM method for morphology analysis of polymer systems. *Polymer* **2011**, *52*, 1278.
12. Geng, X.; Zhai, M. X.; Sun, T.; Meyers, G. Morphology observation of latex particles with scanning transmission electron microscopy by a hydroxyethyl cellulose embedding combined with $RuO_4$ staining method. *Microsc. Microanal.* **2013**, *19*, 319.
13. Klein, T.; Buhr, E.; Frase, C. G. In Advances in Imaging and Electron Physics, Vol. 171; Hawkes, P. W., Ed.; Elsevier: San Diego, CA, **2012**; p. 297.
14. Stokes, D. J.; Baken, E. Electron microscopy of soft nanomaterials. *Imaging Microsc.* **2007**, *9*, 18.
15. Acevedo-Reyes, D.; Perez, M.; Verdu, C.; Bogner, A.; Epicier, T. Characterization of precipitates size distribution: validation of low-voltage STEM. *J. Microsc.* **2008**, *232*, 112.

16. Brodusch, N.; Demers, H.; Gauvin, R. Dark-Field imaging of thin specimens with a forescatter electron detector at low accelerating voltage. *Microsc. Microanal.* **2013**, *19*, 1688.
17. Patel, B.; Watanabe, M. An inexpensive approach for bright-field and dark-field imaging by scanning transmission electron microscopy in scanning electron microscopy. *Microsc. Microanal.* **2014**, *20*, 124.
18. Schneider, C. A.; Rasband, W. S.; Eliceiri, K.W. NIH Image to ImageJ: 25 years of image analysis. *Nat. Methods* **2012**, *9*, 671.
19. Egerton, R. F. Electron Energy-Loss Spectroscopy in the Electron Microscope; Plenum Press: New York, **1996**.
20. Bals, S.; Kabius, B.; Haider, M.; Radmilovic, V.; Kisielowski, C. Annular dark field imaging in a TEM, *Solid State Commun.* **2004**, *130*, 675.
21. Goldstein, J.; Newbury, D. E.; Joy, D. C.; Lyman, C. E.; Echlin, P.; Lifshin, E.; Sawyer, L.; Michael, J. R. Scanning Electron Microscopy and X-Ray Microanalysis. Springer: New York, **2003**.